Fine structure in α decay of even-even nuclei using a finite-range nucleon-nucleon interaction

A. Adel[1,2,*] and T. Alharbi[2]

[1]*Physics Department, Faculty of Science, Cairo University, Giza, Egypt*

[2]*Physics Department, College of Science, Majmaah University, Zulfi, Saudi Arabia*

(Received 24 May 2015; revised manuscript received 29 June 2015; published 21 July 2015)

A systematic study on α-decay fine structure is presented for even-even nuclei in the range $78 \leqslant Z \leqslant 102$. The penetration probability is obtained from the WKB approximation in combination with the Bohr-Sommerfeld quantization condition. The potential barrier is numerically constructed in the well-established double-folding model for both Coulomb and nuclear potentials. A realistic M3Y interaction, based on the G-matrix elements of the Paris NN potential, has been used in the folding calculation. The local approximation for the nondiagonal one-body density matrix in the calculation of the exchange potential was included by using the harmonic oscillator representation of the nondiagonal density matrix of the α particle. The computed partial half-lives and branching ratios are compared with the recent experimental data and they are in good agreement.

DOI: 10.1103/PhysRevC.92.014619 PACS number(s): 23.60.+e, 21.10.Tg, 21.10.Jx

I. INTRODUCTION

α decay is one of the most important decay modes for unstable nuclei and has become a powerful tool to investigate the nuclear structure [1–8] and identify new superheavy elements studied at accelerator centers such as Berkeley, GSI, Dubna, GANIL, and RIKEN [9–12]. In recent years, there has been an increased interest in α decay to excited states of daughter nuclei from both experimental and theoretical sides [13–20]. The half-lives of α emitters provide information on the stability of nuclides, especially for superheavy nuclei, while the decay energies pose a tough test for nuclear-mass models and provide direct information on the excitation energy of final daughter states.

The α-decay process can be divided into two distinct parts: the α clustering of four valence nucleons at the nuclear surface, followed by tunneling of the formed α cluster through the potential barrier. The ground-state to ground-state transition in α decay is only one channel among many possibilities for the decay to other states and this invites use of the term "α fine structure." The population of the excited states in the residual nucleus is usually much weaker than that of the ground state, mainly due to different Q values, reflecting the strong energy dependence of the penetrability of the α particle through the nuclear and Coulomb potential barrier [17]. On the other hand, the population intensity of the excited states also contains important information on their structure.

According to the angular momentum carried by the emitted α particle, there are two groups: favored α transitions with $\ell = 0$ and hindered ones with $\ell \neq 0$. In the spherical or moderately deformed case, α decay in even-even nuclei mainly proceeds between ground 0^+ states, belonging to favored α transitions. In odd-A and odd-odd nuclei, the ground-state spin-parities of parent and daughter nuclei are generally different, leading to the hinderance of the additional centrifugal barrier. Therefore, the transitions between ground states are hindered ones. Theoretically, the hindered α transition is an effective tool to study the properties of α emitters because it is closely related to the internal structure of nuclei.

Many studies on α-decay fine structure for even-even nuclei have been carried out. Denisov and Khudenko [19] calculated the branching ratios and half-lives of α decay to the ground-state rotational bands and high-lying excited states in the framework of the unified model for α decay and α capture (UMADAC). The evaluated branching ratios for $0^+_{\text{g.s.}} \rightarrow 0^+_{\text{g.s.}}, 2^+, 4^+$ α transitions in even-even nuclei agree with the experimental data. Within the framework of the Coulomb and proximity potential model for deformed nuclei (CPPMDN), Santhosh *et al.* [20,21] has done an elaborate study on α-decay fine structure of even-even [20], even-odd [21], and odd-A nuclei [22]. Ni and Ren have used the multichannel cluster model (MCCM) based on the stationary coupled-channel approach for studying the α-decay fine structure observed in heavy even-even nuclei [23,24] and further extended it to odd-A [25] and odd-odd nuclei [16].

Considering the complexity of hindered α decay, it is very interesting to explain the recent available experimental data of hindered α decay based on the favored α-decay theory. In this regard, we have used the Wentzel-Kramers-Brillouin (WKB) framework, reducing α decay to a one-dimensional semiclassical problem [26]. The decay widths for the transitions to various daughter states are evaluated at slightly different decay energies and various centrifugal barriers, ignoring the mixing of channel states during the tunneling. Within this framework, there are some primary studies on α-decay fine structure using simple nuclear potentials such as the popular Woods-Saxon shape and the proximity potential [18–21].

In the present study, α-decay partial half-lives have been determined using microscopic potentials within the semiclassical WKB approximation in combination with the Bohr-Sommerfeld quantization condition for even-even nuclei in the range $78 \leqslant Z \leqslant 102$. The microscopic α-nucleus potential is numerically constructed in the well-established double-folding model for both Coulomb and nuclear potentials. A realistic M3Y interaction, based on the G-matrix elements of the Paris NN potential, has been used in the folding calculation. The main effect of antisymmetrization under exchange of

*aa.ahmed@mu.edu.sa, ahmedadel@sci.cu.edu.eg

 ©2015 American Physical Society

nucleons between the α and daughter nuclei has been included in the folding model through the finite-range exchange part of the NN interaction. The local approximation for the nondiagonal one-body density matrix in the calculation of the exchange potential was included by using the harmonic oscillator representation of the nondiagonal density matrix of the α particle [27–30].

The outline of the paper is as follows. In Sec. II a description of the microscopic nuclear and Coulomb potentials between the α and daughter nuclei is given. The methods for determining the decay width, the penetration probability, the assault frequency, and the preformation probability are also presented. In Sec. III, the calculated results are discussed. Finally, Sec. IV gives a brief conclusion.

II. THEORETICAL FRAMEWORK

The α-decay fine structure can be described using the one-dimensional WKB approximation. In this case, each decay channel is treated as a separate event, and the partial widths for various channels are separately calculated with slightly different decay energies and various centrifugal barriers. The α-decay energy from the various states of a parent nucleus is related to the excitation energy of the different excited states in the daughter nucleus. Thus the Q value for the α transition between the ground level of the parent nucleus and the various levels of the daughter nucleus with excitation energy E_i^* is given by

$$Q_i = Q_{\text{g.s.}\to\text{g.s.}} - E_i^*. \tag{1}$$

The possible values of the angular momentum ℓ for the α-decay transition obey the spin-parity selection rule,

$$|J - J_i| \leqslant \ell \leqslant |J + J_i| \quad \text{and} \quad \frac{\pi_i}{\pi} = (-1)^\ell, \tag{2}$$

where J, π are the spin and parity of the parent nucleus and J_i, π_i are the spin and parity of the daughter nuclei in state i, respectively. In this study, we have done the calculations with the minimal possible values of the angular momentum $\ell_{\min}$ which follows the above two conditions, and are arranged in column 4 of Table I.

The partial α-decay width $\Gamma(Q_i,\ell)$ is mainly determined by the barrier penetration probability (P_α), the assault frequency (ν), and the preformation probability (S_α), $\Gamma(Q_i,\ell) = \hbar\, S_\alpha\, \nu\, P_\alpha$. The barrier penetration probability P_α could be calculated as the barrier transmission coefficient of the well-known WKB approximation, which works well at energies well below the barrier,

$$P_\alpha = \exp\left(-2\int_{R_2}^{R_3} dr \sqrt{\frac{2\,\mu}{\hbar^2}\,|V_T(r) - Q_i|}\right). \tag{3}$$

Here μ is the reduced mass. $R_i (i = 1,2,3)$ are the three turning points for the α-daughter potential barrier where $V_T(r)|_{r=R_i} = Q_i$.

The assault frequency of the α particle, ν, can be expressed as the inverse of the time required to traverse the distance back and forth between the first two turning points, R_1 and R_2, as [31]

$$\nu = T^{-1} = \frac{\hbar}{2\,\mu}\left[\int_{R_1}^{R_2} \frac{dr}{\sqrt{\frac{2\mu}{\hbar^2}\,|V_T(r) - Q_i|}}\right]^{-1}. \tag{4}$$

It is indispensable to evaluate the absolute α-decay half-lives without the inclusion of the α-preformation factor, S_α, which gives the probability that the α particle exists as a recognizable entity inside the nucleus before its emission [8]. It is convenient and applicable to take the constant preformation factor S_α factor for all even-even nuclei, keeping the number of free parameters to a minimum. The motivation for this is clearly shown in Refs. [32–34]. In the present study, we use the preformation probability $S_\alpha = 0.39$ for even-even nuclei as indicated in Ref. [34].

The residual daughter nucleus after disintegration has the most probability of staying in its ground state for even-even nuclei, and the probability of staying in its excited state is relatively much smaller. One particularly interesting hypothesis is that the probability of the residual daughter nucleus to stay in its excited states follows the Boltzmann distribution (BD), $\rho(E_i^*) = \exp(-cE_i^*)$, as Einstein did for molecules with a set of discrete states in 1917 [35]. This procedure has been proven to be successful in describing the fine structure in the α decay. The value of the parameter c is fixed at 2.38 MeV^{-1} as in Ref. [24].

Ultimately, the total α-decay width is given by $\Gamma = \sum_i S_\alpha\, \rho(E_i^*)\, \Gamma(Q_i,\ell)$. The total α-decay half-life, $T_{1/2}$, of the parent nucleus is given in terms of the α decay width, Γ, as

$$T_{1/2} = \frac{\hbar \ln 2}{\Gamma}. \tag{5}$$

The branching ratio (B_i) for α transition to a daughter state i is expressed as

$$B_i = S_\alpha\, \rho(E_i^*)\, \Gamma(Q_i,\ell)/\,\Gamma \times 100\%. \tag{6}$$

Because α decay is understood as a two-body phenomenon involving a core nucleus and an α particle, a reliable input of the α-nucleus interaction potential is required for the quantitative description of α decay. The total interaction potential of the α-core system comprises the nuclear and the Coulomb potentials plus the centrifugal part, and is given by [36]

$$V_T(R) = \lambda\, V_N(R) + V_C(R) + \frac{\hbar^2}{2\,\mu}\frac{\left(\ell + \frac{1}{2}\right)^2}{R^2}, \tag{7}$$

where the renormalization factor λ is the depth of the nuclear potential, R is the separation distance between the mass center of the α particle and the mass center of the core. The latter term in Eq. (7) represents the Langer modified centrifugal potential, μ is the reduced mass of the cluster-core system, and ℓ is the angular momentum carried by the α particle.

The renormalization factor λ, introduced to the nuclear part of the folding potential based on the M3Y interaction, is not an adjustable parameter, but it is determined separately for each decay by applying the Bohr-Sommerfeld quantization condition

$$\int_{R_1}^{R_2} dr \sqrt{\frac{2\,\mu}{\hbar^2}\,|V_T(r) - Q_i|} = (G - \ell + 1)\frac{\pi}{2}, \tag{8}$$

TABLE I. Comparison of computed α-decay half-lives and branching ratios of nuclei with the corresponding experimental values.

Transition	E_d^* (keV)	Q_α^{expt} (MeV)	$\ell_{\min}$	$T_{1/2}^{\text{expt}}$ (s)	$T_{1/2}^{\text{calc}}$ (s)	B^{expt} (%)	B^{calc} (%)
$^{174}\text{Pt} \rightarrow {}^{170}\text{Os}$							
$0^+ \rightarrow 0^+$	0	6.1830	0	1.20×10^{0}	9.98×10^{-1}	99.46	98.34
$0^+ \rightarrow 2^+$	286.7	5.8963	2	2.22×10^{2}	3.06×10^{1}	0.54	1.66
$^{176}\text{Pt} \rightarrow {}^{172}\text{Os}$							
$0^+ \rightarrow 0^+$	0	5.8850	0	1.58×10^{1}	1.65×10^{1}	99.75	97.19
$0^+ \rightarrow 2^+$	228.0	5.6570	2	6.33×10^{3}	3.39×10^{2}	0.25	2.81
$^{178}\text{Pt} \rightarrow {}^{174}\text{Os}$							
$0^+ \rightarrow 0^+$	0	5.5729	0	5.18×10^{2}	4.05×10^{2}	94.56	94.27
$0^+ \rightarrow 2^+$	158.7	5.4142	2	9.00×10^{3}	4.63×10^{3}	5.44	5.73
$^{180}\text{Hg} \rightarrow {}^{176}\text{Pt}$							
$0^+ \rightarrow 0^+$	0	6.2585	0	5.39×10^{0}	3.63×10^{0}	99.87	97.39
$0^+ \rightarrow 2^+$	263.0	5.9955	2	9.92×10^{3}	8.89×10^{1}	0.05	2.17
$0^+ \rightarrow 0^+$	443.0	5.8155	0	6.81×10^{3}	2.95×10^{2}	0.08	0.43
$^{182}\text{Hg} \rightarrow {}^{178}\text{Pt}$							
$0^+ \rightarrow 0^+$	0	5.9960	0	7.22×10^{1}	4.31×10^{1}	99.19	93.84
$0^+ \rightarrow 2^+$	170.7	5.8253	2	1.24×10^{4}	4.75×10^{2}	0.58	5.75
$0^+ \rightarrow 0^+$	422.0	5.5740	0	3.01×10^{4}	3.80×10^{3}	0.24	0.40
$^{184}\text{Hg} \rightarrow {}^{180}\text{Pt}$							
$0^+ \rightarrow 0^+$	0	5.6620	0	2.47×10^{3}	1.33×10^{3}	99.44	93.70
$0^+ \rightarrow 2^+$	153.0	5.5090	2	6.17×10^{5}	1.42×10^{4}	0.40	6.19
$0^+ \rightarrow 0^+$	478.0	5.1840	0	1.54×10^{6}	3.64×10^{5}	0.16	0.11
$^{186}\text{Pb} \rightarrow {}^{182}\text{Hg}$							
$0^+ \rightarrow 0^+$	0	6.4700	0	1.21×10^{1}	3.69×10^{0}	99.73	97.20
$0^+ \rightarrow (0^+)$	328.0	6.1420	0	6.04×10^{3}	8.38×10^{1}	0.20	2.01
$0^+ \rightarrow 2^+$	351.8	6.1182	2	1.61×10^{4}	2.01×10^{2}	0.07	0.79
$^{188}\text{Pb} \rightarrow {}^{184}\text{Hg}$							
$0^+ \rightarrow 0^+$	0	6.1090	0	2.73×10^{2}	1.09×10^{2}	98.91	98.72
$0^+ \rightarrow 2^+$	367.0	5.7420	2	2.85×10^{5}	9.72×10^{3}	0.09	0.47
$0^+ \rightarrow 0^+$	375.0	5.7340	2	2.70×10^{4}	5.58×10^{3}	1.00	0.81
$^{190}\text{Pb} \rightarrow {}^{186}\text{Hg}$							
$0^+ \rightarrow 0^+$	0	5.6970	0	1.78×10^{4}	7.85×10^{3}	99.90	99.79
$0^+ \rightarrow 2^+$	409.0	5.2880	2	2.09×10^{7}	1.88×10^{6}	0.09	0.16
$0^+ \rightarrow 0^+$	532.0	5.1650	0	1.27×10^{8}	4.71×10^{6}	0.01	0.05
$^{190}\text{Po} \rightarrow {}^{186}\text{Pb}$							
$0^+ \rightarrow 0^+$	0	7.6930	0	2.55×10^{-3}	1.26×10^{-3}	96.40	99.35
$0^+ \rightarrow (0^+)$	536.0	7.1570	0	7.45×10^{-2}	7.25×10^{-2}	3.30	0.50
$0^+ \rightarrow (0^+)$	655.0	7.0380	0	8.20×10^{-1}	1.91×10^{-1}	0.30	0.15
$^{192}\text{Po} \rightarrow {}^{188}\text{Pb}$							
$0^+ \rightarrow 0^+$	0	7.3200	0	3.31×10^{-2}	1.87×10^{-2}	97.86	99.72
$0^+ \rightarrow (0^+)$	568.0	6.7520	0	2.25×10^{0}	2.02×10^{0}	1.44	0.25
$0^+ \rightarrow (0^+)$	767.0	6.5530	0	4.60×10^{0}	1.21×10^{1}	0.70	0.03
$^{194}\text{Po} \rightarrow {}^{190}\text{Pb}$							
$0^+ \rightarrow 0^+$	0	6.9870	0	4.22×10^{-1}	2.53×10^{-1}	99.76	99.94
$0^+ \rightarrow 0^+$	658.0	6.3290	0	1.78×10^{2}	9.37×10^{1}	0.24	0.06
$^{196}\text{Po} \rightarrow {}^{192}\text{Pb}$							
$0^+ \rightarrow 0^+$	0	6.6580	0	6.17×10^{0}	4.05×10^{0}	99.92	99.99
$0^+ \rightarrow 0^+$	767.0	5.8910	0	7.87×10^{3}	2.80×10^{4}	7.84×10^{-2}	2.48×10^{-3}
$^{198}\text{Po} \rightarrow {}^{194}\text{Pb}$							
$0^+ \rightarrow 0^+$	0	6.3096	0	1.86×10^{2}	9.86×10^{1}	99.99	99.99
$0^+ \rightarrow 0^+$	930.7	5.3789	0	1.40×10^{7}	2.87×10^{6}	1.33×10^{-3}	4.04×10^{-4}
$^{198}\text{Rn} \rightarrow {}^{194}\text{Po}$							
$0^+ \rightarrow 0^+$	0	7.3490	0	6.55×10^{-2}	8.84×10^{-2}	99.93	98.11
$0^+ \rightarrow 2^+$	319	7.0300	2	9.29×10^{1}	2.21×10^{0}	7.04×10^{-2}	1.89×10^{0}
$^{200}\text{Rn} \rightarrow {}^{196}\text{Po}$							
$0^+ \rightarrow 0^+$	0	7.0433	0	1.05×10^{0}	9.98×10^{-1}	99.99	99.52
$0^+ \rightarrow 2^+$	463	6.5803	2	1.75×10^{4}	1.14×10^{2}	6.02×10^{-3}	3.02×10^{-1}
$0^+ \rightarrow 0^+$	558	6.4853	0	1.30×10^{4}	1.51×10^{2}	8.06×10^{-3}	1.82×10^{-1}

TABLE I. (*Continued.*)

Transition	E_d^* (keV)	Q_α^{expt} (MeV)	$\ell_{\min}$	$T_{1/2}^{\text{expt}}$ (s)	$T_{1/2}^{\text{calc}}$ (s)	B^{expt} (%)	B^{calc} (%)
$^{202}\text{Rn} \rightarrow {}^{198}\text{Po}$							
$0^+ \rightarrow 0^+$	0	6.7737	0	1.24×10^{1}	9.71×10^{0}	99.99	99.99
$0^+ \rightarrow 0^+$	816	5.9577	0	6.93×10^{5}	3.14×10^{4}	1.79×10^{-3}	4.73×10^{-3}
$^{208}\text{Rn} \rightarrow {}^{204}\text{Po}$							
$0^+ \rightarrow 0^+$	0	6.2607	0	2.36×10^{3}	1.05×10^{3}	99.95	99.99
$0^+ \rightarrow 2^+$	684.3	5.5764	2	5.04×10^{6}	3.88×10^{6}	4.68×10^{-2}	5.62×10^{-3}
$^{210}\text{Rn} \rightarrow {}^{206}\text{Po}$							
$0^+ \rightarrow 0^+$	0	6.1589	0	9.00×10^{3}	2.79×10^{3}	99.99	99.99
$0^+ \rightarrow 2^+$	700.7	5.4582	2	1.60×10^{8}	1.56×10^{7}	5.62×10^{-3}	3.58×10^{-3}
$^{212}\text{Rn} \rightarrow {}^{208}\text{Po}$							
$0^+ \rightarrow 0^+$	0	6.3850	0	1.43×10^{3}	2.66×10^{2}	99.95	99.99
$0^+ \rightarrow 2^+$	686.5	5.6985	2	2.87×10^{6}	7.86×10^{5}	5.0×10^{-2}	6.97×10^{-3}
$^{218}\text{Rn} \rightarrow {}^{214}\text{Po}$							
$0^+ \rightarrow 0^+$	0	7.2625	0	3.50×10^{-2}	5.31×10^{-2}	99.87	99.93
$0^+ \rightarrow 2^+$	609.3	6.6532	2	2.76×10^{1}	1.80×10^{1}	1.27×10^{-1}	7.25×10^{-2}
$^{220}\text{Rn} \rightarrow {}^{216}\text{Po}$							
$0^+ \rightarrow 0^+$	0	6.4046	0	5.57×10^{1}	9.82×10^{1}	99.89	99.95
$0^+ \rightarrow 2^+$	549.7	5.8549	2	4.88×10^{4}	5.69×10^{4}	1.14×10^{-1}	4.87×10^{-2}
$^{222}\text{Rn} \rightarrow {}^{218}\text{Po}$							
$0^+ \rightarrow 0^+$	0	5.5903	0	3.31×10^{5}	6.35×10^{5}	99.92	99.98
$0^+ \rightarrow 2^+$	511	5.0793	2	4.24×10^{8}	9.01×10^{8}	7.80×10^{-2}	2.18×10^{-2}
$0^+ \rightarrow$?	675	4.9153	0	6.61×10^{10}	5.13×10^{9}	5.00×10^{-4}	2.62×10^{-3}
$^{222}\text{Ra} \rightarrow {}^{218}\text{Rn}$							
$0^+ \rightarrow 0^+$	0	6.6790	0	3.92×10^{1}	5.74×10^{1}	96.94	98.90
$0^+ \rightarrow 2^+$	324.3	6.3547	2	1.25×10^{3}	2.46×10^{3}	3.05×10^{0}	1.10×10^{0}
$0^+ \rightarrow (4^+)$	653.1	6.0259	4	9.27×10^{5}	3.20×10^{5}	4.10×10^{-3}	3.95×10^{-3}
$0^+ \rightarrow (3^-)$	796.9	5.8821	3	9.27×10^{5}	7.29×10^{5}	4.10×10^{-3}	1.24×10^{-3}
$0^+ \rightarrow (3^-)$	840.2	5.8388	3	9.05×10^{5}	1.20×10^{6}	4.20×10^{-3}	6.84×10^{-4}
$^{224}\text{Ra} \rightarrow {}^{220}\text{Rn}$							
$0^+ \rightarrow 0^+$	0	5.7889	0	3.31×10^{5}	6.06×10^{5}	94.92	98.32
$0^+ \rightarrow 2^+$	241	5.5479	2	6.20×10^{6}	2.06×10^{7}	5.06×10^{0}	1.67×10^{0}
$0^+ \rightarrow 4^+$	533.7	5.2552	4	4.42×10^{9}	3.87×10^{9}	7.10×10^{-3}	4.51×10^{-3}
$0^+ \rightarrow 1^-$	645.4	5.1435	1	4.13×10^{9}	2.95×10^{9}	7.60×10^{-3}	4.57×10^{-3}
$0^+ \rightarrow (3^-)$	663	5.1259	3	1.05×10^{10}	1.04×10^{10}	3.00×10^{-3}	1.24×10^{-3}
$^{226}\text{Ra} \rightarrow {}^{222}\text{Rn}$							
$0^+ \rightarrow 0^+$	0	4.8706	0	5.38×10^{10}	1.24×10^{11}	93.83	98.16
$0^+ \rightarrow 2^+$	186.2	4.6844	2	8.20×10^{11}	4.32×10^{12}	6.16×10^{0}	1.83×10^{0}
$0^+ \rightarrow 4^+$	448.4	4.4222	4	7.77×10^{14}	1.57×10^{15}	6.50×10^{-3}	2.77×10^{-3}
$0^+ \rightarrow 1^-$	600.7	4.2699	1	5.05×10^{15}	3.98×10^{15}	1.00×10^{-3}	7.67×10^{-4}
$0^+ \rightarrow 3^-$	635.5	4.2351	3	1.87×10^{16}	2.15×10^{16}	2.70×10^{-4}	1.31×10^{-4}
$^{216}\text{Th} \rightarrow {}^{212}\text{Ra}$							
$0^+ \rightarrow 0^+$	0	8.0720	0	2.61×10^{-2}	9.95×10^{-3}	99.46	99.89
$0^+ \rightarrow 2^+$	628.3	7.4437	2	4.81×10^{0}	2.15×10^{0}	5.40×10^{-1}	1.09×10^{-1}
$^{226}\text{Th} \rightarrow {}^{222}\text{Ra}$							
$0^+ \rightarrow 0^+$	0	6.4509	0	2.43×10^{3}	4.04×10^{3}	75.54	84.56
$0^+ \rightarrow 2^+$	111.1	6.3398	2	8.04×10^{3}	2.29×10^{4}	2.28×10^{1}	1.16×10^{1}
$0^+ \rightarrow 1^-$	242.1	6.2088	1	1.46×10^{6}	6.19×10^{4}	1.26×10^{0}	3.17×10^{0}
$0^+ \rightarrow 4^+$	301.4	6.1495	4	9.81×10^{5}	6.92×10^{5}	1.87×10^{-1}	2.47×10^{-1}
$0^+ \rightarrow 3^-$	317.3	6.1336	3	8.90×10^{5}	3.76×10^{5}	2.06×10^{-1}	4.39×10^{-1}
$0^+ \rightarrow (5^-)$	473.8	5.9771	5	7.97×10^{8}	1.28×10^{7}	2.30×10^{-4}	8.99×10^{-3}
$0^+ \rightarrow (0^+)$	914	5.5369	0	5.39×10^{8}	1.38×10^{8}	3.40×10^{-4}	3.02×10^{-4}
$0^+ \rightarrow 2^+$	1024.9	5.4260	2	1.08×10^{9}	1.07×10^{9}	1.70×10^{-4}	3.01×10^{-5}
$^{228}\text{Th} \rightarrow {}^{224}\text{Ra}$							
$0^+ \rightarrow 0^+$	0	5.5201	0	8.36×10^{7}	1.61×10^{8}	72.14	84.49
$0^+ \rightarrow 2^+$	84.4	5.4357	2	2.22×10^{8}	8.84×10^{8}	27.18	12.66
$0^+ \rightarrow 1^-$	216	5.3041	1	1.44×10^{10}	3.50×10^{9}	4.20×10^{-1}	2.36×10^{0}
$0^+ \rightarrow 4^+$	250.8	5.2693	4	2.66×10^{10}	3.43×10^{10}	2.27×10^{-1}	2.23×10^{-1}
$0^+ \rightarrow (3)^-$	290.4	5.2297	3	1.59×10^{11}	2.68×10^{10}	3.80×10^{-2}	2.60×10^{-1}
$0^+ \rightarrow (5)^-$	433.1	5.0870	5	6.03×10^{14}	1.27×10^{12}	9.99×10^{-6}	3.97×10^{-3}

TABLE I. (*Continued.*)

Transition	E_d^* (keV)	Q_α^{expt} (MeV)	$\ell_{\min}$	$T_{1/2}^{\text{expt}}$ (s)	$T_{1/2}^{\text{calc}}$ (s)	B^{expt} (%)	B^{calc} (%)
$0^+ \to (6^+)$	479.3	5.0408	6	2.41×10^{14}	8.30×10^{12}	2.50×10^{-5}	5.43×10^{-4}
$0^+ \to 0^+$	916.3	4.6038	0	3.35×10^{14}	1.31×10^{14}	1.80×10^{-5}	1.26×10^{-5}
$0^+ \to (2^+)$	992.7	4.5274	2	1.28×10^{15}	9.09×10^{14}	4.70×10^{-6}	1.52×10^{-6}
$^{230}\text{Th} \to {}^{226}\text{Ra}$							
$0^+ \to 0^+$	0	4.7698	0	3.12×10^{12}	7.77×10^{12}	76.41	85.98
$0^+ \to 2^+$	67.7	4.7021	2	1.02×10^{13}	4.32×10^{13}	23.44	13.23
$0^+ \to 4^+$	211.5	4.5583	4	1.98×10^{15}	2.05×10^{15}	1.20×10^{-1}	2.01×10^{-1}
$0^+ \to 1^-$	253.7	4.5161	1	7.93×10^{15}	6.91×10^{14}	3.00×10^{-2}	5.40×10^{-1}
$0^+ \to 3^-$	321.5	4.4483	3	2.45×10^{17}	6.39×10^{15}	9.71×10^{-4}	5.00×10^{-2}
$0^+ \to 6^+$	416.5	4.3533	6	2.97×10^{19}	7.62×10^{17}	8.01×10^{-6}	3.36×10^{-4}
$0^+ \to 5^-$	446.3	4.3235	5	2.31×10^{19}	3.97×10^{17}	1.03×10^{-5}	6.03×10^{-4}
$0^+ \to 0^+$	824.6	3.9452	0	7.00×10^{19}	3.90×10^{19}	3.41×10^{-6}	2.57×10^{-6}
$0^+ \to 2^+$	873.7	3.8961	2	1.70×10^{20}	2.12×10^{20}	1.40×10^{-6}	4.23×10^{-7}
$^{232}\text{Th} \to {}^{228}\text{Ra}$							
$0^+ \to 0^+$	0	4.0816	0	5.65×10^{17}	2.06×10^{18}	78.22	88.91
$0^+ \to 2^+$	63.8	4.0178	2	2.04×10^{18}	1.43×10^{19}	21.71	11.00
$0^+ \to 4^+$	204.7	3.8769	4	6.40×10^{20}	1.27×10^{21}	6.90×10^{-2}	8.96×10^{-2}
$^{228}\text{U} \to {}^{224}\text{Th}$							
$0^+ \to 0^+$	0	6.8040	0	8.03×10^{2}	1.01×10^{3}	69.97	81.29
$0^+ \to 2^+$	93	6.7110	2	1.95×10^{3}	4.43×10^{3}	28.81	14.95
$0^+ \to 1^-$	246	6.5580	1	8.53×10^{4}	1.38×10^{4}	6.59×10^{-1}	3.38×10^{0}
$0^+ \to 4^+$	280	6.5240	4	9.93×10^{4}	1.11×10^{5}	5.66×10^{-1}	3.86×10^{-1}
$^{232}\text{U} \to {}^{228}\text{Th}$							
$0^+ \to 0^+$	0	5.41363	0	3.19×10^{9}	6.85×10^{9}	68.15	81.40
$0^+ \to 2^+$	57.8	5.35583	2	6.89×10^{9}	2.75×10^{10}	31.55	17.75
$0^+ \to 4^+$	186.9	5.22673	4	7.25×10^{11}	6.84×10^{11}	3.00×10^{-1}	5.30×10^{-1}
$0^+ \to 1^-$	327.9	5.08573	1	3.53×10^{13}	9.13×10^{11}	6.16×10^{-3}	2.87×10^{-1}
$0^+ \to 6^+$	377.9	5.03573	6	4.26×10^{15}	1.03×10^{14}	5.10×10^{-5}	2.27×10^{-3}
$0^+ \to 3^-$	396	5.01763	3	4.53×10^{15}	6.96×10^{12}	4.80×10^{-5}	3.22×10^{-2}
$0^+ \to 5^-$	519.1	4.89453	5	3.88×10^{15}	2.87×10^{14}	5.60×10^{-5}	5.89×10^{-4}
$0^+ \to 0^+$	831.4	4.58223	0	1.04×10^{16}	2.70×10^{15}	2.10×10^{-5}	3.05×10^{-5}
$0^+ \to 2^+$	874.6	4.53903	2	5.58×10^{16}	1.06×10^{16}	3.90×10^{-6}	7.01×10^{-6}
$^{234}\text{U} \to {}^{230}\text{Th}$							
$0^+ \to 0^+$	0	4.8577	0	1.09×10^{13}	2.43×10^{13}	71.38	82.68
$0^+ \to 2^+$	53.2	4.8045	2	2.73×10^{13}	1.05×10^{14}	28.42	16.90
$0^+ \to 4^+$	174.1	4.6836	4	3.87×10^{15}	3.23×10^{15}	2.00×10^{-1}	4.17×10^{-1}
$0^+ \to 1^-$	508.2	4.3495	1	1.94×10^{19}	2.21×10^{17}	4.00×10^{-5}	2.83×10^{-3}
$0^+ \to 0^+$	634.9	4.2228	0	2.98×10^{19}	2.15×10^{18}	2.60×10^{-5}	2.18×10^{-4}
$0^+ \to 2^+$	677.6	4.1801	2	1.11×10^{20}	9.32×10^{18}	7.00×10^{-6}	4.54×10^{-5}
$^{236}\text{U} \to {}^{232}\text{Th}$							
$0^+ \to 0^+$	0	4.5729	0	9.99×10^{14}	2.79×10^{15}	73.89	82.86
$0^+ \to 2^+$	49.5	4.5234	2	2.84×10^{15}	1.23×10^{16}	25.96	16.74
$0^+ \to 4^+$	162.3	4.4106	4	4.93×10^{17}	3.99×10^{17}	1.50×10^{-1}	4.00×10^{-1}
$0^+ \to 6^+$	333.4	4.2395	6	5.28×10^{20}	9.85×10^{19}	1.40×10^{-4}	1.09×10^{-3}
$^{238}\text{U} \to {}^{234}\text{Th}$							
$0^+ \to 0^+$	0	4.2700	0	1.78×10^{17}	7.41×10^{17}	78.94	84.35
$0^+ \to 2^+$	49.6	4.2204	2	6.71×10^{17}	3.63×10^{18}	20.98	15.37
$0^+ \to 4^+$	163	4.1070	4	1.81×10^{20}	1.51×10^{20}	7.79×10^{-2}	2.84×10^{-1}
$^{230}\text{Pu} \to {}^{226}\text{U}$							
$0^+ \to 0^+$	0	7.1800	0	1.26×10^{2}	2.32×10^{2}	81.00	77.59
$0^+ \to 2^+$	59	7.1210	2	5.37×10^{2}	7.01×10^{2}	19.00	22.41
$^{232}\text{Pu} \to {}^{228}\text{U}$							
$0^+ \to 0^+$	0	6.7160	0	1.35×10^{4}	1.77×10^{4}	66.37	78.68
$0^+ \to 2^+$	59	6.6570	2	2.67×10^{4}	5.69×10^{4}	33.63	21.32
$^{234}\text{Pu} \to {}^{230}\text{U}$							
$0^+ \to 0^+$	0	6.3100	0	7.73×10^{5}	1.17×10^{6}	68.06	77.23
$0^+ \to 2^+$	51.7	6.2583	2	1.67×10^{6}	3.70×10^{6}	31.54	21.65
$0^+ \to 4^+$	169.5	6.1405	4	1.32×10^{8}	5.44×10^{7}	3.98×10^{-1}	1.12×10^{0}

TABLE I. (*Continued.*)

Transition	E_d^* (keV)	Q_α^{expt} (MeV)	$\ell_{\min}$	$T_{1/2}^{\text{expt}}$ (s)	$T_{1/2}^{\text{calc}}$ (s)	B^{expt} (%)	B^{calc} (%)
$^{236}\text{Pu} \rightarrow {}^{232}\text{U}$							
$0^+ \rightarrow 0^+$	0	5.8671	0	1.31×10^{8}	1.91×10^{8}	69.01	77.46
$0^+ \rightarrow 2^+$	47.6	5.8195	2	2.93×10^{8}	6.17×10^{8}	30.76	21.45
$0^+ \rightarrow 4^+$	156.5	5.7106	4	3.92×10^{10}	9.58×10^{9}	2.30×10^{-1}	1.08×10^{0}
$0^+ \rightarrow 6^+$	322.7	5.5444	6	4.88×10^{12}	7.26×10^{11}	1.85×10^{-3}	9.68×10^{-3}
$0^+ \rightarrow 8^+$	540.7	5.3264	8	6.94×10^{14}	2.78×10^{14}	1.30×10^{-5}	1.53×10^{-5}
$0^+ \rightarrow 1^-$	563.2	5.3039	1	3.47×10^{13}	4.21×10^{11}	2.60×10^{-4}	9.60×10^{-3}
$0^+ \rightarrow 0^+$	691.5	5.1756	0	1.55×10^{13}	2.27×10^{12}	5.79×10^{-4}	1.32×10^{-3}
$0^+ \rightarrow 2^+$	734.6	5.13247	2	6.94×10^{14}	7.86×10^{12}	1.30×10^{-5}	3.47×10^{-4}
$0^+ \rightarrow 5^-$	746.8	5.1203	5	3.67×10^{15}	1.00×10^{14}	2.46×10^{-6}	2.65×10^{-5}
$0^+ \rightarrow 4^+$	833.5	5.0336	4	1.50×10^{16}	1.43×10^{14}	5.99×10^{-7}	1.52×10^{-5}
$0^+ \rightarrow 2^+$	866.9	5.0002	2	7.45×10^{14}	6.09×10^{13}	1.21×10^{-5}	3.30×10^{-5}
$0^+ \rightarrow (0^+)$	927.3	4.9398	0	6.78×10^{14}	8.80×10^{13}	1.33×10^{-5}	1.99×10^{-5}
$0^+ \rightarrow (2^+)$	967.6	4.8995	2	5.89×10^{14}	3.06×10^{14}	1.53×10^{-5}	5.21×10^{-6}
$^{240}\text{Pu} \rightarrow {}^{236}\text{U}$							
$0^+ \rightarrow 0^+$	0	5.2558	0	2.84×10^{11}	6.10×10^{11}	72.81	78.88
$0^+ \rightarrow 2^+$	45.2	5.2106	2	7.64×10^{11}	2.14×10^{12}	27.10	20.28
$0^+ \rightarrow 4^+$	149.5	5.1063	4	2.46×10^{14}	4.06×10^{13}	8.40×10^{-2}	8.40×10^{-1}
$0^+ \rightarrow 6^+$	309.8	4.9460	6	1.95×10^{16}	4.33×10^{15}	1.06×10^{-3}	5.44×10^{-3}
$0^+ \rightarrow 8^+$	522.3	4.7335	8	4.50×10^{17}	2.82×10^{18}	4.60×10^{-5}	5.13×10^{-6}
$0^+ \rightarrow 1^-$	687.6	4.5682	1	1.04×10^{18}	5.34×10^{16}	2.00×10^{-5}	1.85×10^{-4}
$0^+ \rightarrow 3^-$	744.2	4.5116	3	1.59×10^{21}	4.07×10^{17}	1.30×10^{-8}	2.13×10^{-5}
$0^+ \rightarrow 0^+$	919.2	4.3366	0	3.51×10^{19}	3.45×10^{18}	5.90×10^{-7}	1.68×10^{-6}
$0^+ \rightarrow (2^+)$	958	4.2978	2	4.14×10^{20}	1.35×10^{19}	5.00×10^{-8}	9.93×10^{-5}
$0^+ \rightarrow (2^+)$	960	4.2958	2	6.90×10^{20}	1.41×10^{19}	3.00×10^{-8}	1.30×10^{-5}
$0^+ \rightarrow 1^-$	967	4.2888	1	6.90×10^{20}	1.09×10^{19}	3.00×10^{-8}	1.51×10^{-6}
$^{238}\text{Cm} \rightarrow {}^{234}\text{Pu}$							
$0^+ \rightarrow 0^+$	0	6.6700	0	3.24×10^{5}	2.01×10^{5}	69.53	76.03
$0^+ \rightarrow 2^+$	46	6.6240	2	7.38×10^{5}	5.72×10^{5}	30.47	23.97
$^{240}\text{Cm} \rightarrow {}^{236}\text{Pu}$							
$0^+ \rightarrow 0^+$	0	6.3978	0	3.29×10^{6}	3.43×10^{6}	71.07	75.15
$0^+ \rightarrow 2^+$	44.6	6.3532	2	8.10×10^{6}	9.98×10^{6}	28.87	23.32
$0^+ \rightarrow 4^+$	147.5	6.2503	4	4.50×10^{9}	1.21×10^{8}	5.20×10^{-2}	1.51×10^{0}
$0^+ \rightarrow 6^+$	305.8	6.0920	6	1.67×10^{10}	6.28×10^{9}	1.40×10^{-2}	2.03×10^{-2}
$^{242}\text{Cm} \rightarrow {}^{238}\text{Pu}$							
$0^+ \rightarrow 0^+$	0	6.2156	0	1.90×10^{7}	2.51×10^{7}	74.05	75.50
$0^+ \rightarrow 2^+$	44.1	6.1715	2	5.43×10^{7}	7.43×10^{7}	25.91	23.04
$0^+ \rightarrow 4^+$	146	6.06956	4	4.02×10^{10}	9.45×10^{8}	3.50×10^{-2}	1.43×10^{0}
$0^+ \rightarrow 6^+$	303.4	5.9122	6	3.06×10^{11}	5.30×10^{10}	4.60×10^{-3}	1.78×10^{-2}
$0^+ \rightarrow 8^+$	513.6	5.7020	8	7.04×10^{13}	1.39×10^{13}	2.00×10^{-5}	4.19×10^{-5}
$0^+ \rightarrow 1^-$	605.1	5.6105	1	5.63×10^{12}	5.78×10^{10}	2.50×10^{-4}	8.14×10^{-3}
$0^+ \rightarrow 3^-$	661.3	5.5543	3	1.12×10^{14}	3.27×10^{11}	1.26×10^{-5}	1.26×10^{-3}
$0^+ \rightarrow 5^-$	763.2	5.4524	5	6.40×10^{15}	7.70×10^{12}	2.20×10^{-7}	4.25×10^{-5}
$0^+ \rightarrow 0^+$	941.4	5.2742	0	3.91×10^{13}	5.59×10^{12}	3.60×10^{-5}	3.89×10^{-5}
$0^+ \rightarrow 1^-$	962.7	5.2529	1	1.25×10^{15}	9.33×10^{12}	1.13×10^{-6}	2.22×10^{-5}
$0^+ \rightarrow 2^+$	983	5.2326	2	8.28×10^{14}	1.87×10^{13}	1.70×10^{-6}	1.06×10^{-5}
$0^+ \rightarrow 2^+$	1028.6	5.1870	2	3.80×10^{14}	3.73×10^{13}	3.70×10^{-6}	4.77×10^{-6}
$0^+ \rightarrow (4^+)$	1125.8	5.0898	4	4.54×10^{15}	6.57×10^{14}	3.10×10^{-7}	2.16×10^{-7}
$0^+ \rightarrow 0^+$	1228.7	4.9869	0	2.56×10^{15}	4.82×10^{14}	5.50×10^{-7}	2.33×10^{-7}
$0^+ \rightarrow 2^+$	1264.7	4.9513	2	2.71×10^{15}	1.55×10^{15}	5.20×10^{-7}	6.67×10^{-8}
$^{244}\text{Cf} \rightarrow {}^{240}\text{Cm}$							
$0^+ \rightarrow 0^+$	0	7.3289	0	2.20×10^{3}	2.25×10^{3}	74.65	72.98
$0^+ \rightarrow (2^+)$	38	7.2909	2	6.47×10^{3}	5.58×10^{3}	25.35	27.02
$^{246}\text{Cf} \rightarrow {}^{242}\text{Cm}$							
$0^+ \rightarrow 0^+$	0	6.8616	0	1.62×10^{5}	1.87×10^{5}	79.25	73.25
$0^+ \rightarrow 2^+$	42.1	6.8195	2	6.24×10^{5}	5.04×10^{5}	20.59	24.71
$0^+ \rightarrow 4^+$	137	6.7246	4	8.57×10^{7}	4.98×10^{6}	1.50×10^{-1}	2.01×10^{0}
$0^+ \rightarrow 6^+$	288	6.5736	6	8.03×10^{8}	1.95×10^{8}	1.60×10^{-2}	3.64×10^{-2}

TABLE I. (*Continued.*)

Transition	E_d^* (keV)	Q_α^{expt} (MeV)	$\ell_{\min}$	$T_{1/2}^{\text{expt}}$ (s)	$T_{1/2}^{\text{calc}}$ (s)	B^{expt} (%)	B^{calc} (%)
$^{248}\text{Cf} \rightarrow {}^{244}\text{Cm}$							
$0^+ \rightarrow 0^+$	0	6.3615	0	3.60×10^{7}	3.74×10^{7}	80	74.89
$0^+ \rightarrow 2^+$	43	6.3185	2	1.47×10^{8}	1.08×10^{8}	19.6	23.54
$0^+ \rightarrow 4^+$	142.3	6.2192	4	7.20×10^{9}	1.28×10^{9}	4.00×10^{-1}	1.57×10^{0}
$^{250}\text{Cf} \rightarrow {}^{246}\text{Cm}$							
$0^+ \rightarrow 0^+$	0	6.1284	0	5.00×10^{8}	5.36×10^{8}	82.60	75.51
$0^+ \rightarrow 2^+$	42.9	6.0855	2	2.41×10^{9}	1.59×10^{9}	17.11	23.04
$0^+ \rightarrow 4^+$	142	5.9864	4	1.46×10^{11}	2.04×10^{10}	2.83×10^{-1}	1.43×10^{0}
$0^+ \rightarrow 6^+$	293	5.8354	6	5.90×10^{12}	1.12×10^{12}	7.00×10^{-3}	1.84×10^{-2}
$^{248}\text{Fm} \rightarrow {}^{244}\text{Cf}$							
$0^+ \rightarrow 0^+$	0	8.0020	0	4.86×10^{1}	4.35×10^{1}	79.91	72.61
$0^+ \rightarrow 2^+$	41	7.9610	2	1.94×10^{2}	1.05×10^{2}	20.09	27.39
$^{250}\text{Fm} \rightarrow {}^{246}\text{Cf}$							
$0^+ \rightarrow 0^+$	0	7.5570	0	2.40×10^{3}	1.79×10^{3}	83.33	73.97
$0^+ \rightarrow 2^+$	44	7.5130	2	1.20×10^{4}	4.59×10^{3}	16.67	26.03
$^{252}\text{Fm} \rightarrow {}^{248}\text{Cf}$							
$0^+ \rightarrow 0^+$	0	7.1527	0	1.09×10^{5}	7.11×10^{4}	84.01	72.51
$0^+ \rightarrow 2^+$	41.5	7.1112	2	6.09×10^{5}	1.85×10^{5}	15.00	25.29
$0^+ \rightarrow 4^+$	137.8	7.0149	4	9.42×10^{6}	1.75×10^{6}	9.70×10^{-1}	2.15×10^{0}
$0^+ \rightarrow 6^+$	285	6.8677	6	3.97×10^{8}	5.92×10^{7}	2.30×10^{-2}	4.52×10^{-2}
$^{252}\text{No} \rightarrow {}^{250}\text{Fm}$							
$0^+ \rightarrow 0^+$	0	8.5490	0	4.78×10^{0}	3.50×10^{0}	75.00	72.47
$0^+ \rightarrow 2^+$	44	8.5050	2	1.44×10^{1}	8.34×10^{0}	25.00	27.53
$^{256}\text{No} \rightarrow {}^{252}\text{Fm}$							
$0^+ \rightarrow 0^+$	0	8.5810	0	3.36×10^{0}	2.43×10^{0}	87.04	72.90
$0^+ \rightarrow 2^+$	46.6	8.5344	2	2.26×10^{1}	5.87×10^{0}	12.96	27.10

where the global quantum number $G = 20\,(N > 126)$ and $G = 18\,(82 < N \leqslant 126)$ [36]. In Ref. [31], the half-lives are found to be sensitive to the implementation of this condition in the WKB approach, which fixes the depth of the double-folding nuclear potential λ. The application of this condition is correct for the case of spherical daughter nucleus because the periodicity of α-particle motion fulfills.

The nuclear part of the potential $V_N(R)$ consists of two terms, the direct $V_D(R)$ and the exchange $V_{\text{Ex}}(R)$ terms. The direct part of the interaction between two colliding nuclei and the equation describing the Coulomb interaction have similar forms involving only diagonal elements of the density matrix [37,38]

$$V_D(R) = \int \mathrm{d}\vec{r}_1 \int \mathrm{d}\vec{r}_2 \rho_\alpha(\vec{r}_1)\, \upsilon_D(s)\, \rho_d(\vec{r}_2), \tag{9}$$

where s is the relative distance between a constituent nucleon in the α particle and one in the daughter nucleus. $\rho_\alpha(\vec{r}_1)$ and $\rho_d(\vec{r}_2)$ are, respectively, the density distributions of the α particle and the residual daughter nucleus.

The matter density distribution of the α particle is a standard Gaussian form [37], namely,

$$\rho_\alpha(r) = 0.4229\, \exp(-0.7024\, r^2). \tag{10}$$

The matter density distribution for the daughter nucleus can be described by the spherically symmetric Fermi function [26,36],

$$\rho_d(r) = \frac{\rho_0}{1 + \exp\left(\frac{r - R_0}{a}\right)}, \tag{11}$$

where the value of ρ_0 has been fixed by integrating the matter density distribution equivalent to the mass number of the residual daughter nucleus A_d. The half-density radius, R_0, and the diffuseness parameter, a, are given by [39,40]

$$R_0 = 1.07 A_d^{1/3}\ \text{fm}, \quad a = 0.54\ \text{fm}. \tag{12}$$

The exchange potential accounts for the knock-on exchange of nucleons between the interacting nuclei. The exchange term is, in general, nonlocal. However, an accurate local approximation can be obtained by treating the relative motion locally as a plane wave [27,30]

$$V_{\text{Ex}}(R) = \int d\vec{r}_1 \int d\vec{r}_2 \rho_\alpha(\vec{r}_1, \vec{r}_1 + \vec{s})\, \rho_d(\vec{r}_2, \vec{r}_2 - \vec{s}) \times \upsilon_{\text{Ex}}(s)\, \exp\left[\frac{i\vec{k}(R)\cdot\vec{s}}{M}\right]. \tag{13}$$

Here $k(R)$ is the relative-motion momentum given by

$$k^2(R) = \frac{2\mu}{\hbar^2}[E_{\text{c.m.}} - V_N(R) - V_C(R)], \tag{14}$$

where μ is the reduced mass for the reacting nuclei, and $E_{\text{c.m.}}$ is the center-of-mass energy. $V_N(R) = V_D(R) + V_{\text{Ex}}(R)$ and $V_C(R)$ are the total nuclear and Coulomb potentials,

respectively. The folded potential is energy dependent and nonlocal through its exchange term and contains a self-consistency problem because the relative-motion momentum, $k(R)$, depends upon the total nuclear potential, $V_N(R) = V_D(R) + V_{\rm Ex}(R)$, itself. This problem is solved by the iteration method. The exact treatment of the nonlocal exchange term is complicated numerically, but one may obtain an equivalent *local* potential by using a realistic localized expression for the nonlocal density matrix (DM) [27,30]

$$\rho(\vec{r},\vec{r}+\vec{s}) \simeq \rho\left(\vec{r}+\frac{\vec{s}}{2}\right)\hat{j}_1\left[k_{\rm eff}\left(\vec{r}+\frac{\vec{s}}{2}\right)s\right], \qquad (15)$$

with

$$\hat{j}_1(x) = 3\,j_1(x)/x = 3(\sin x - x\,\cos x)/x^3. \qquad (16)$$

The α particle is a unique case where a simple Gaussian can reproduce very well its ground-state density [37]. Assuming four nucleons to occupy the lowest $s\frac{1}{2}$ harmonic oscillator shell in ^{4}He, one obtains exactly the nondiagonal ground-state DM for the α particle as [30]

$$\rho_\alpha(\vec{r},\vec{r}+\vec{s}) \simeq \rho_\alpha\left(\left|\vec{r}+\frac{\vec{s}}{2}\right|\right)\exp\left(-\frac{s^2}{4\,b_\alpha^2}\right), \qquad (17)$$

where b_α is equal to 1.1932 fm.

To accelerate the convergence of the density matrix expansion, Campi and Bouyssy [41] have suggested to choose, for a spherically symmetric ground-state density, the local Fermi momentum, $k_{\rm eff}(r)$, in the following form:

$$k_{\rm eff}(r) = \left\{\frac{5}{3\rho(r)}\left[\tau(r) - \frac{1}{4}\nabla^2\rho(r)\right]\right\}^{1/2}. \qquad (18)$$

Using the extended Thomas-Fermi approximation, the kinetic energy density is then given by

$$\tau(r) = \frac{3}{5}\left(\frac{3\pi^2}{2}\right)^{2/3}\rho(r)^{5/3} + \frac{1}{3}\nabla^2\rho(r) + \frac{1}{36}\frac{|\vec{\nabla}\rho(r)|^2}{\rho(r)}. \qquad (19)$$

The first term in this expression stands for Thomas-Fermi approximation while the other two terms represent the surface correction.

One easily obtains the self-consistent and local exchange potential $V_{\rm Ex}$ as [30]

$$V_{\rm Ex}(R) = 4\,\pi\int_0^\infty {\rm d}s\, s^2\,\upsilon_{\rm Ex}(s)\,j_0(k(R)s/M) \times\int {\rm d}\vec{y}\,\rho_d(|\vec{y}-\vec{R}|)\,\hat{j}_1(k_{\rm eff}(|\vec{y}-\vec{R}|)s) \times\rho_\alpha(y)\exp\left(-\frac{s^2}{4\,b_\alpha^2}\right). \qquad (20)$$

The exchange potential, Eq. (20), can then be evaluated by an iterative procedure which converges very fast.

The realistic M3Y-Paris effective NN interaction is used in our present calculations and it has the form [37,42]

$$\upsilon_D(s) = \left[11061.625\,\frac{e^{-4s}}{4\,s} - 2537.5\,\frac{e^{-2.5s}}{2.5\,s}\right], \qquad (21)$$

$$\upsilon_{\rm Ex}(s) = \left[-1524.25\,\frac{e^{-4s}}{4\,s} - 518.75\,\frac{e^{-2.5s}}{2.5\,s} - 7.8474\,\frac{e^{-0.7072s}}{0.7072\,s}\right], \qquad (22)$$

III. RESULTS AND DISCUSSION

The α-decay half-lives of even-even nuclei in the range $78 \leqslant Z \leqslant 102$ from the ground state of the parent nuclei to the ground and the excited states of the daughter nuclei have been systematically investigated. For the case of even-even nuclei, α decay mainly proceeds from ground state 0^+ to ground state 0^+. Actually, the even-even parent nuclei can also decay from their ground states to the excited states of the rotational band in the corresponding daughter nuclei. The decay to the excited states of the daughter nucleus is the unfavored case because they are strongly hindered as compared with the ground-state ones. The influences of the excitation energy as well as the angular momentum of the α particle have been included in calculating the penetration probability of the α particle through the Coulomb barrier.

We have calculated the microscopic α-nucleus potential in the well-established double-folding model. A realistic M3Y-Paris NN interaction with a finite-range exchange part has been used. This type of NN interaction produces the nuclear matter saturation curve and the energy dependence of the nucleon-nucleus optical potential model. Moreover, the main effect of antisymmetrization under exchange of nucleons between the α and the daughter nuclei has been included in the folding model through the finite-range exchange part of the NN interaction. This is a novel development in the fine-structure calculations of α decays.

Figure 1(a) represents the comparison of the calculated branching ratios with the available experimental data for the α decay of ^{226}Ra from its 0^+ ground state to low-lying members of the favored rotational band of ^{222}Rn. As additional information, the spin-parity and excitation energy of the final daughter states are listed. One sees that the calculated branching ratios for the α decay of ^{226}Ra have values close to their experimental counterparts. On examining the branching ratio values it is seen that the highest branching ratios are to the 0^+ states followed by the 2^+ states. The α transitions to the remaining states are strongly hindered. Figure 1(b) shows the histogram representing the hindrance factor of ^{226}Ra nucleus from its 0^+ ground state to various states of ^{222}Rn.

Table I displays the comparison of our evaluations with the available experimental data for branching ratios and half-lives of α decay to the ground-state rotational bands as well as the high-lying excited states of even-even nuclei in the mass regions $174 \leqslant A \leqslant 256$ and $78 \leqslant Z \leqslant 102$. The first column of Table I denotes the decay from the ground state of the parent nuclei to the ground state and various excited states of the daughter nuclei. The spin-parity values enclosed in

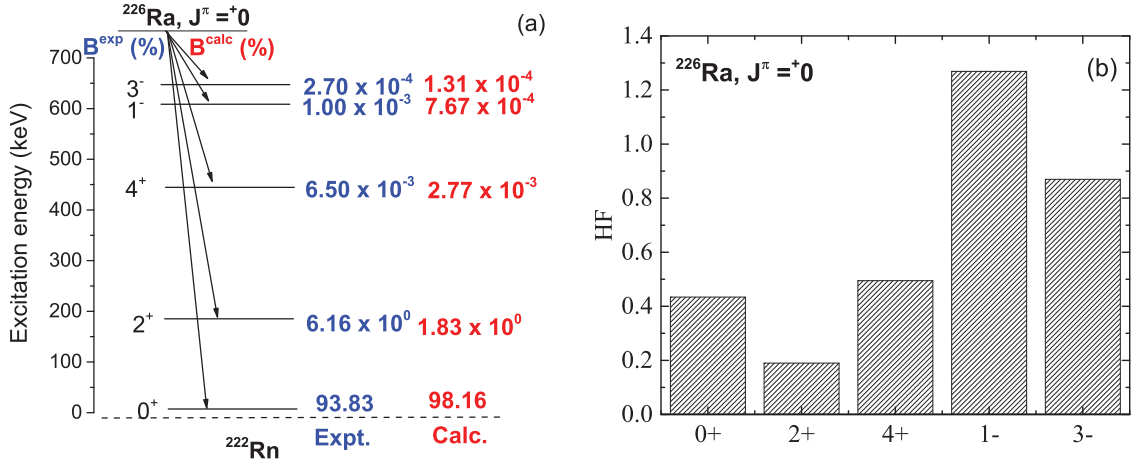

FIG. 1. (Color online) (a) Comparison of the calculated branching ratios with the available experimental data for the α decay of ^{226}Ra from its 0^+ ground state to various states of ^{222}Rn. The experimental data are shown in blue and the calculated results are shown in red. (b) Histogram showing the hindrance factor of ^{226}Ra nucleus.

parentheses denote those values are inaccurate. The Q value and the excitation spectrum in the daughter nuclei are very crucial in the α-decay study. So their values are set by experiment. The excitation energies of the daughter states and the experimental Q values of the corresponding decay channels are listed in the second and third columns. Their values are taken from the NuDat database [43]. The minimal possible values of the orbital angular momentum of the α particle $\ell_{\min}$ are listed in column 4. They are calculated according to the spin-parity selection rule of Eq. (2). The experimental and calculated values of the partial α-decay half-lives for various daughter states are listed in columns 5 and 6. The experimental partial half-lives are evaluated from NuDat database by using total α half-lives and intensity to different states of daughter nucleus. The last two columns are the same as columns 5 and 6 but for branching ratios.

As shown in Table I, most of the calculated half-lives are in good agreement with the corresponding experimental data even though the experimental half-lives span over a wide range from 10^{-2} to 10^{20} s. Transitions showing large deviations between calculated and experimental values correspond to less intense transitions having large uncertainty in the experimental value or belong to the transition between undefined angular momentum states. For example, the ground-state Q value of ^{234}Pu is 6.310 ± 0.005 MeV and will give the α-decay half-life $T_{1/2}^{\text{calc}} = 1.17^{+0.07}_{-0.06} \times 10^6$ s. An uncertainty of 1 MeV in the Q value corresponds to an uncertainty of α-decay half-life ranging from 10^3 to 10^5 times in the heavy element region [44]. A precise measurement with α emitters in present experimental facilities would be most welcome to test the validity of the present study and will give us valuable guidance to improve α-decay studies.

Figure 2(a) represents a Geiger-Nuttall plot of the ground-state to ground-state α decays for the isotopic sequences of Pt, Po, and Th. A comparison between the calculated values and the corresponding values of the Geiger-Nuttall law with parameters obtained from Ref. [45] is presented. It is clear that the calculated values of α-decay half-lives follow the

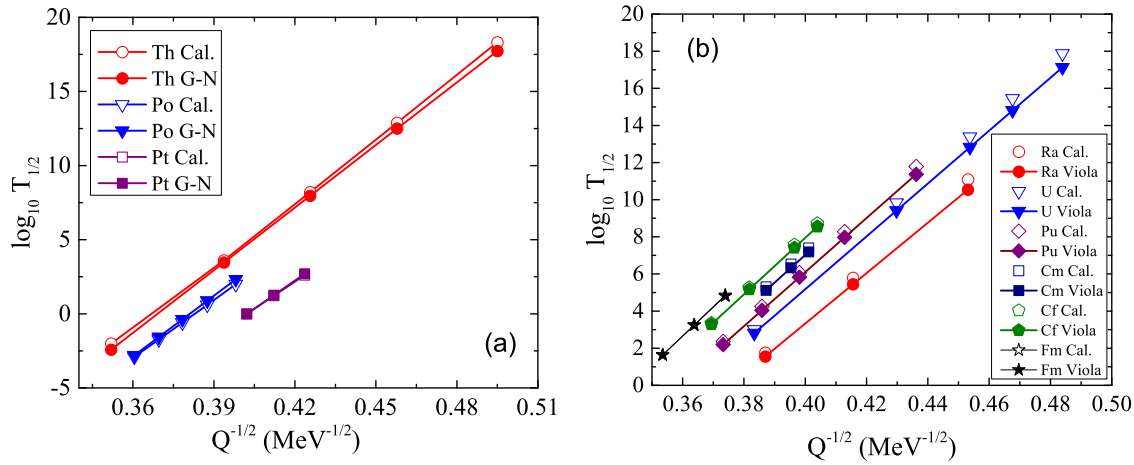

FIG. 2. (Color online) Geiger-Nuttall plots of ground-state to ground-state α decays of some even-even nuclei. (a) Comparison between the calculated values and the corresponding values of Geiger-Nuttall law with parameters obtained from Ref. [45]. (b) Comparison between the calculated values and the corresponding values of Viola-Seaborg formula with parameters obtained from Ref. [46].

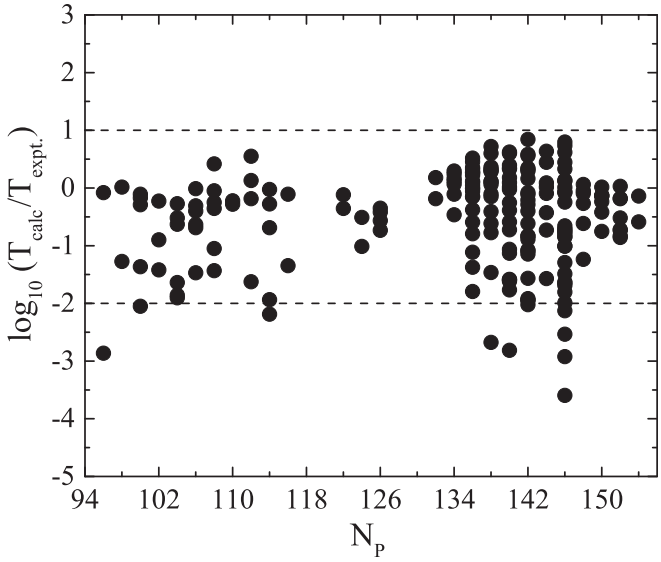

FIG. 3. Deviation of the calculated partial half-lives with the corresponding experimental data for all transitions.

Geiger-Nuttall law which states that there is a linear relationship between the logarithm of α-decay half-lives and the reciprocal of the square root of decay energies. Viola and Seaborg generalized the Geiger-Nuttall law with additional adjustable parameters and proposed a new relation about the logarithm of half-life, α-decay energy, and charge number of the parent nucleus. Figure 2(b) represents a comparison between the calculated values of the ground-state to ground-state α decays for the isotopic sequences of Ra, U, Pu, Cm, Cf, and Fm with the corresponding values calculated from the Viola-Seaborg formula with parameters obtained from Ref. [46]. A good agreement is achieved between the calculated values and the values from the Viola-Seaborg formula.

Figure 3 displays the deviations of calculated α-decay half-lives from the experimental data as a function of the neutron number N of the parent nucleus for the entire transitions. It is clear that for most of the transitions, the deviation of calculated α-decay half-lives with the corresponding experimental data lie within the order 2. This means that most of the calculated α-decay half-lives are in good agreement with the experimental data for even-even nuclei. Because the constant preformation factor cannot completely describe the detailed features of nuclear structure, one can notice, for some transitions, that there is a slight deviation from the corresponding experimental data.

Finally, to show the effective strength of our calculations, we have evaluated the standard deviation (σ) of both half-life and branching ratio using the following expression:

$$\sigma = \sqrt{\frac{1}{n-1}\sum_{i=1}^{n}\left[\log\left(\frac{T_{1/2}^{\text{calc}}}{T_{1/2}^{\text{expt}}}\right)\right]^2}. \quad (23)$$

The obtained standard deviation of half-life for all transitions is 0.977 and that for branching ratio is 0.833.

IV. SUMMARY AND CONCLUSION

A systematic study of the α-decay fine structure in even-even nuclei has been performed. The calculations cover the isotopic chains from Pt to No in the mass regions $174 \leqslant A \leqslant 256$ and $78 \leqslant Z \leqslant 102$. We have treated α decay as a one-dimensional problem and worked in the framework of the well-known WKB semiclassical approximation in combination with the Bohr-Sommerfeld quantization condition. The potential barrier is numerically constructed in the well-established double-folding model for both Coulomb and nuclear potentials. A realistic M3Y-Paris NN interaction with a finite-range exchange part has been used. In contrast to the other traditional semiclassical approximations which ignore the main effect of antisymmetrization under exchange of nucleons between the α and the daughter nuclei, the present calculations take into account such an effect in the folding model through the finite-range exchange part of the NN interaction. We have also assumed that the excitation spectrum in daughter nuclei satisfies the Boltzmann distribution, which is very similar to the hypothesis of Einstein for atomic spectrum.

On the whole, there exists good agreement between experiment and theory for the fine structure in the studied nuclei. The evaluated standard deviations for the half-life and branching ratio are 0.977 and 0.833, respectively. Although a good agreement between experiment and theory is achieved, there are still some open problems. For example, the mechanism of α-particle preformation and how it varies with different excited states of daughter nuclei instead of a constant. This is worth further investigation.

ACKNOWLEDGMENTS

A. Adel is very grateful to Professor M. Ismail (Cairo University) for valuable discussions. The authors would like to thank the deanship of scientific research, Majmaah University, Saudi Arabia, for funding this work under Project No. 28-A-1435.

[1] W. M. Seif, Phys. Rev. C **91**, 014322 (2015).
[2] M. Ismail and A. Adel, Phys. Rev. C **90**, 064624 (2014).
[3] M. Ismail and A. Adel, Phys. Rev. C **89**, 034617 (2014).
[4] Yibin Qian, Zhongzhou Ren, and Dongdong Ni, Phys. Rev. C **89**, 024318 (2014).
[5] D. Bucurescu and N. V. Zamfir, Phys. Rev. C **87**, 054324 (2013).
[6] M. Ismail and A. Adel, Phys. Rev. C **88**, 054604 (2013).
[7] M. Ismail and A. Adel, Nucl. Phys. A **912**, 18 (2013).
[8] M. Ismail and A. Adel, Phys. Rev. C **86**, 014616 (2012).
[9] Yu. Ts. Oganessian *et al.*, Phys. Rev. Lett. **104**, 142502 (2010).
[10] Yu. Ts. Oganessian *et al.*, Phys. Rev. C **87**, 054621 (2013).
[11] Yu. Ts. Oganessian *et al.*, Phys. Rev. C **74**, 044602 (2006).
[12] S. Hofmann *et al.*, Eur. Phys. J. A **10**, 5 (2001).
[13] D. S. Delion and A. Dumitrescu, At. Data Nucl. Data Tables **101**, 1 (2015).
[14] A. N. Andreyev *et al.*, Phys. Rev. C **90**, 044312 (2014).

[15] A. Lopez-Martens *et al.*, Eur. Phys. J. A **50**, 132 (2014).
[16] D. Ni and Z. Ren, Phys. Rev. C **87**, 027602 (2013).
[17] D. Bucurescu and N. V. Zamfir, Phys. Rev. C **86**, 067306 (2012).
[18] Y. Z. Wang, J. Z. Gu, J. M. Dong, and B. B. Peng, Eur. Phys. J. A **44**, 287 (2010).
[19] V. Yu. Denisov and A. A. Khudenko, Phys. Rev. C **80**, 034603 (2009).
[20] K. P. Santhosh, S. Sahadevan, and J. G. Joseph, Nucl. Phys. A **850**, 34 (2011).
[21] K. P. Santhosh, J. G. Joseph, and B. Priyanka, Nucl. Phys. A **877**, 1 (2012).
[22] K. P. Santhosh and J. G. Joseph, Phys. Rev. C **86**, 024613 (2012).
[23] D. Ni and Z. Ren, Phys. Rev. C **81**, 064318 (2010).
[24] D. Ni and Z. Ren, Phys. Rev. C **83**, 067302 (2011).
[25] D. Ni and Z. Ren, Phys. Rev. C **86**, 054608 (2012).
[26] M. Ismail, A. Y. Ellithi, M. M. Botros, and A. Adel, Phys. Rev. C **81**, 024602 (2010).
[27] B. Sinha, Phys. Rep. **20**, 1 (1975).
[28] M. Ismail, F. Salah, and M. M. Osman, Phys. Rev. C **54**, 3308 (1996).
[29] M. Ismail, M. M. Osman, and F. Salah, Phys. Rev. C **60**, 037603 (1999).
[30] Dao T. Khoa, Phys. Rev. C **63**, 034007 (2001).
[31] N. G. Kelkar and H. M. Castaneda, Phys. Rev. C **76**, 064605 (2007).
[32] B. Buck, A. C. Merchant, and S. M. Perez, Phys. Rev. C **51**, 559 (1995).
[33] B. Buck, A. C. Merchant, and S. M. Perez, At. Data Nucl. Data Tables **54**, 53 (1993).
[34] D. Ni and Z. Ren, Phys. Rev. C **81**, 024315 (2010).
[35] A. Einstein, Physik. Z. **18**, 121 (1927).
[36] C. Xu and Z. Ren, Nucl. Phys. A **753**, 174 (2005).
[37] G. R. Satchler and W. G. Love, Phys. Rep. **55**, 183 (1979).
[38] M. Ismail and A. Adel, Phys. Rev. C **84**, 034610 (2011).
[39] C. Xu and Z. Ren, Phys. Rev. C **74**, 014304 (2006).
[40] C. Xu and Z. Ren, Phys. Rev. C **73**, 041301(R) (2006).
[41] X. Campi and A. Bouyssy, Phys. Lett. B **73**, 263 (1978).
[42] M. E. Brandan and G. R. Satchler, Phys. Rep. **285**, 143 (1997).
[43] NuDat2.6, Nuclear Structure and Decay Data, available from: http://www.nndc.bnl.gov/nudat2/.
[44] E. O. Fiset and J. R. Nix, Nucl. Phys. A **193**, 647 (1972).
[45] B. Buck, A. C. Merchant, and S. M. Perez, Phys. Rev. Lett. **65**, 2975 (1990).
[46] T. Dong and Z. Ren, Eur. Phys. J. A **26**, 69 (2005).